Journal of Non-Newtonian Fluid Mechanics

J. Non-Newtonian Fluid Mech. 101 (2001) 55–76

www.elsevier.com/locate/jnnfm

Study of steady pipe and channel flows of a single-mode Phan-Thien–Tanner fluid

Manuel A. Alves [a], Fernando T. Pinho [b,*], Paulo J. Oliveira [c]

[a] *Departamento de Engenharia Química, CEFT, Faculdade de Engenharia, Universidade do Porto, Rua Roberto Frias, 4200-465 Porto, Portugal*

[b] *Centro de Estudos de Fenómenos de Transporte, DEMEGI, Faculdade de Engenharia, Universidade do Porto, Rua Roberto Frias, 4200-465 Porto, Portugal*

[c] *Departamento de Engenharia Electromecânica, Universidade da Beira Interior, 6201-001 Covilhã, Portugal*

Received 7 May 2001; received in revised form 13 September 2001

Abstract

Analytical solutions are derived for the steady state channel and pipe flows of viscoelastic fluids obeying the complete single-mode Phan-Thien–Tanner (PTT) constitutive equation with a linear stress coefficient in the absence of a solvent viscosity contribution. The results include the profiles of all relevant stresses, the axial velocity and the viscosity across the gap. The three material functions of the single-mode PTT model in steady Couette flow are also given and it is shown that the conditions of the maximum point in the shear stress versus shear rate curve are related to the conditions for existence of steady state solutions in the channel and pipe flows. The range of model parameters for which a classical steady solution exists is established. © 2001 Elsevier Science B.V. All rights reserved.

Keywords: Phan-Thien–Tanner constitutive equation; Analytical solution; Constitutive instability; Pipe flow; Channel flow

1. Introduction

Using considerations of nonaffine movement of the network junctions relative to the continuum medium, the complete Phan-Thien–Tanner (PTT) constitutive equation was developed from the Lodge–Yamamoto network theory by Phan-Thien and Tanner [1] and Phan-Thien [2] to model the rheological behaviour of polymer melts. For an isothermal flow this rheological equation of state can be written in a compact form as

$$Y(\mathrm{Tr}\,\boldsymbol{\tau})\boldsymbol{\tau} + \lambda \overset{\square}{\boldsymbol{\tau}} = 2\eta \boldsymbol{D}, \leq \tag{1}$$

* Corresponding author. Fax: +351-225081763.
E-mail addresses: mmalves@fe.up.pt (M.A. Alves), fpinho@fe.up.pt (F.T. Pinho), pjpo@ubi.pt (P.J. Oliveira).

PII: S0377-0257(01)00159-8

where $\boldsymbol{\tau}$ and $\boldsymbol{D}$ are the extra stress and rate of deformation tensors, λ is a relaxation time and η is the constant viscosity coefficient; $\overset{\square}{\boldsymbol{\tau}}$ is the Gordon–Schowalter convected derivative usually defined as

$$\overset{\square}{\boldsymbol{\tau}} \cong \frac{D\tau}{Dt} - \boldsymbol{\tau} \cdot \nabla \boldsymbol{u} - \nabla \boldsymbol{u}^{\mathrm{T}} \cdot \boldsymbol{\tau} + \xi(\boldsymbol{\tau} \cdot \boldsymbol{D} + \boldsymbol{D} \cdot \boldsymbol{\tau}). \tag{2}$$

This derivative is akin to Oldroyd's upper convected derivative (the first three terms on the right-hand-side of Eq. (2)) if we use an effective velocity gradient $\boldsymbol{L}$ instead of the velocity gradient $\nabla \boldsymbol{u}$, i.e.

$$\overset{\square}{\boldsymbol{\tau}} = \frac{D\boldsymbol{\tau}}{Dt} - \boldsymbol{\tau} \cdot \boldsymbol{L} - \boldsymbol{L}^{\mathrm{T}} \cdot \boldsymbol{\tau}, \tag{3}$$

where the effective velocity gradient $\boldsymbol{L}$ is defined by

$$\boldsymbol{L} \equiv \nabla \boldsymbol{u} - \xi \boldsymbol{D}. \tag{4}$$

Thus, parameter ξ accounts for the slip between the molecular network and the continuum medium. A simplified version of the above model is the so-called simplified Phan-Thien–Tanner (SPTT) equation where $\xi = 0$.

The stress coefficient function has an exponential form [2]:

$$Y(\mathrm{Tr}\, \boldsymbol{\tau}) = \phi(T) f(\mathrm{Tr}\, \boldsymbol{\tau}) = \phi(T) \exp\left(\frac{\varepsilon\lambda}{\eta} \mathrm{Tr}\, \boldsymbol{\tau}\right), \tag{5}$$

which can be accurately linearised for small molecular deformations as occurs in weak flows (according to the flow classification of Tanner and Huilgol [3]), such as the channel, pipe and pure Couette steady flows dealt with in this paper. The linearised stress coefficient function to be used in this work is then given by

$$f(\mathrm{Tr}\, \boldsymbol{\tau}) = 1 + \frac{\varepsilon\lambda}{\eta} \mathrm{Tr}\, \boldsymbol{\tau}, \tag{6}$$

which was the form proposed in the original paper of Phan-Thien and Tanner [1]. Furthermore, as this is an isothermal problem, the thermal function $\phi(T)$ in Eq. (5) is set to 1 following Phan-Thien [2].

The stress coefficient function introduces a new parameter ε which imposes an upper limit to the elongational viscosity which becomes inversely proportional to ε. If this extensional parameter is set to 0, then $f(\mathrm{Tr}\, \boldsymbol{\tau}) = 1$ and the Johnson–Segalman (JS) constitutive equation, used for dilute polymer solutions, is recovered [4].

Viscoelastic flows through pipes and channels are relevant in the polymer processing industry [5] and simple analytical solutions are preferred to the use of complex calculation routines. Analytical solutions give physical insight into flow phenomena and besides can be used to check results of numerical calculations. Recently, a series of analytical solutions for the simplified PTT model in duct flows have been derived by the authors: channel and pipe flows by Oliveira and Pinho [6] using both the linear and the exponential forms of the stress coefficient function; the corresponding forced convection problem for imposed wall heat flux by Pinho and Oliveira [7]; and the annular flow solution by Pinho and Oliveira [8], the two latter works involving only the linear form of the stress coefficient. Similar solutions for pipe and channel flows with the Giesekus model are presented by Choi et al. [9], Lim and Schowalter [10] and Schleiniger and Weinacht [11]. For the eight-constant Oldroyd model fluid Deiber and Santa Cruz [12] derived the velocity profile in pipe flow and similar results for a channel appear in Kolkka et al. [13] for JS fluid with added Newtonian solvent. An implicit analytical solution for the JS fluid in axisymmetric pipe flow was given earlier by Van Schaftingen and Crochet [14], who expressed the velocity and stress variations in terms of the local shear rates. Pipe and channel flow solutions for simpler viscoelastic models, such as the upper convective Maxwell model (UCM), are identical to the corresponding Newtonian solutions presented by Shah and London [15]. For solutions of purely viscous generalised Newtonian fluids the works of Bird et al. [16] and Skelland [17] can be consulted.

The above viscoelastic solutions pertain to single-mode constitutive equations. For very accurate predictions of many real viscoelastic fluids multi-mode models are usually required but, nevertheless, solutions for single-mode constitutive equations give physical insight, are adequate in many practical situations and provide means for validating numerical methods.

This work extends the original paper of Oliveira and Pinho [6] by presenting analytical solutions for steady, laminar pipe and channel flows of the full single-mode PTT having a linear form of the stress coefficient. The constitutive equation does not include a solvent viscosity contribution, the common situation for polymer melts, and an investigation of the influence of the various model parameters upon the flow characteristics is carried out. For the exponential form of the stress coefficient a similar analytical solution could not be obtained. Prior to the presentation of the solutions for the pipe and channel flows, the material functions of the PTT model in steady shear flow are presented and discussed.

2. Material functions in steady plane shear flow

We consider a simple plane shear flow aligned with x (shear rate $\dot{\gamma} = u_{,y}$) and we seek expressions for the three material functions, namely the viscometric viscosity $\mu(\dot{\gamma})$, and the first and second normal stress difference coefficients, $\Psi_1(\dot{\gamma})$ and $\Psi_2(\dot{\gamma})$, respectively.

For this simple viscometric flow the constitutive Eq. (1) reduces to

$$f(\boldsymbol{\tau}_{ii})\boldsymbol{\tau}_{xx} = \lambda(2-\xi)\dot{\gamma}\boldsymbol{\tau}_{xy}, \tag{7}$$

$$f(\boldsymbol{\tau}_{ii})\boldsymbol{\tau}_{yy} = -\lambda\xi\dot{\gamma}\boldsymbol{\tau}_{xy}, \tag{8}$$

$$f(\boldsymbol{\tau}_{ii})\boldsymbol{\tau}_{xy} = \eta\dot{\gamma} + \lambda\left(1-\frac{\xi}{2}\right)\dot{\gamma}\boldsymbol{\tau}_{yy} - \frac{\lambda\xi}{2}\dot{\gamma}\boldsymbol{\tau}_{xx}, \tag{9}$$

where the function $f(\boldsymbol{\tau}_{ii})$ is given by Eq. (6). The trace of the stress tensor is $\boldsymbol{\tau}_{ii} = \boldsymbol{\tau}_{xx} + \boldsymbol{\tau}_{yy}$ and the ratio of Eqs. (7) and (8) shows the relationship between both normal stresses to be

$$\boldsymbol{\tau}_{yy} = -\frac{\xi}{2-\xi}\boldsymbol{\tau}_{xx}. \tag{10}$$

Using Eq. (7) for $\boldsymbol{\tau}_{xy}$ and Eq. (10) for $\boldsymbol{\tau}_{yy}$, which are introduced into Eq. (9), we arrive after some algebraic manipulations at the following cubic equation:

$$\boldsymbol{\tau}_{xx}^3 + a_1\boldsymbol{\tau}_{xx}^2 + a_2\boldsymbol{\tau}_{xx} + a_3 = 0, \tag{11}$$

where

$$a_1 = \frac{\eta(2-\xi)}{\varepsilon\lambda(1-\xi)}, \tag{12a}$$

$$a_2 = \frac{\eta^2(2-\xi)^3\dot{\gamma}^2\xi}{4\varepsilon^2(1-\xi)^2} + \frac{\eta^2(2-\xi)^2}{4\varepsilon^2\lambda^2(1-\xi)^2}, \tag{12b}$$

$$a_3 = -\frac{\eta^3(2-\xi)^3\dot{\gamma}^2}{4\varepsilon^2\lambda(1-\xi)^2}. \tag{12c}$$

The real solution of this cubic equation can be expressed as

$$\boldsymbol{\tau}_{xx}(\dot{\gamma}) = \sqrt[3]{-\frac{\beta}{2} + \sqrt{\frac{\beta^2}{4} + \frac{\alpha^3}{27}}} + \sqrt[3]{-\frac{\beta}{2} - \sqrt{\frac{\beta^2}{4} + \frac{\alpha^3}{27}}} - \frac{a_1}{3}, \tag{13}$$

with

$$\alpha = a_2 - \frac{a_1^2}{3}, \tag{14a}$$

$$\beta = a_3 - \frac{a_1 a_2}{3} + \frac{2a_1^3}{27}, \tag{14b}$$

and is an explicit function of the shear rate $\dot{\gamma}$ and the model parameters, albeit in a complex way.

The shear stress is given by Eq. (9), written in terms of $\boldsymbol{\tau}_{xx}$ for compactness

$$\boldsymbol{\tau}_{xy}(\dot{\gamma}) = \frac{\eta - \lambda\xi\boldsymbol{\tau}_{xx}}{1 + [2\varepsilon\lambda(1-\xi)/\eta(2-\xi)]\boldsymbol{\tau}_{xx}}\dot{\gamma}, \tag{15}$$

and the material functions are then obtained from their definitions:

$$\mu(\dot{\gamma}) \equiv \frac{\boldsymbol{\tau}_{xy}}{\dot{\gamma}} = \frac{\eta - \lambda\xi\boldsymbol{\tau}_{xx}}{1 + [2\varepsilon\lambda(1-\xi)/\eta(2-\xi)]\boldsymbol{\tau}_{xx}}, \tag{16}$$

$$\Psi_1(\dot{\gamma}) \equiv \frac{\boldsymbol{\tau}_{xx} - \boldsymbol{\tau}_{yy}}{\dot{\gamma}^2} = \frac{2\boldsymbol{\tau}_{xx}}{(2-\xi)\dot{\gamma}^2}, \tag{17}$$

$$\Psi_2(\dot{\gamma}) \equiv \frac{\boldsymbol{\tau}_{yy} - \boldsymbol{\tau}_{zz}}{\dot{\gamma}^2} = \frac{-\xi\boldsymbol{\tau}_{xx}}{(2-\xi)\dot{\gamma}^2}. \tag{18}$$

Different, but equivalent, expressions for these material functions are also given by Xue et al. [18] who, however, have not analysed the shear stress–shear rate behaviour in detail. We can separate such analysis into two cases which exhibit markedly different behaviour: $\xi = 0$ and $\xi \neq 0$.

For $\xi = 0$, the SPTT model is recovered and, as indicated by Eq. (18), it cannot predict a non-zero second normal stress coefficient. The SPTT model has a shear-thinning behaviour in both the viscometric viscosity and $\Psi_1(\dot{\gamma})$ at intermediate and high shear rates, but constant coefficients at low shear rates. This is well shown by the full lines of the shear and normal stress profiles in log–log coordinates of Figs. 1 and 2: for the shear stress the slope of the full lines at low shear rates is equal to 1 (constant viscosity), but decreases as $\dot{\gamma}$ increases (shear-thinning); similarly, for $\boldsymbol{\tau}_{xx}$ the slope is equal to 2 at low shear rates

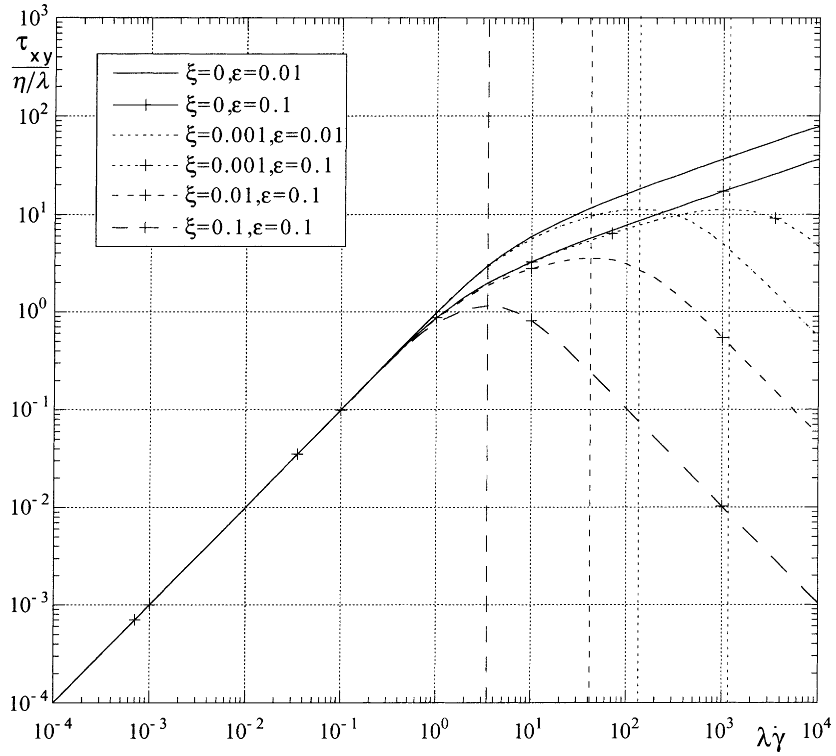

Fig. 1. Variation of the shear stress with shear rate in steady Couette flow for a PTT fluid with linear stress coefficient. Vertical lines: $\lambda\dot{\gamma}_c$ of Eq. (19).

(constant Ψ_1) and decreases as the shear rate is increased (shear-thinning). Note that at intermediate and high shear rates the variation of the stresses with $\dot{\gamma}$ is independent of the value of ε for low values of ε. This is a known result from the literature as ε basically affects extensional flow properties provided ε is small [4]. This characteristic of ε remains if ε is smaller than ξ in the case of the full PTT fluid ($\xi \neq 0$).

For $\xi \neq 0$, the constitutive equation exhibits a non-monotonic behaviour for the shear stress similar to that of a pure JS fluid [19,20] and, as shown by the dashed lines in Figs. 1 and 2, all shear flow characteristics are affected by the value of the slip parameter ξ. Above a critical shear rate ($\dot{\gamma}_c$) defined by the point where the shear stress attains its maximum value, shear-thinning intensity becomes so strong that the slope $\mathrm{d}\ln\mu/\mathrm{d}\ln\dot{\gamma}$ becomes smaller than -1. This critical shear rate depends on both ξ, and ε, and was found here to be given by

$$\lambda\dot{\gamma}_c = \frac{\varepsilon(1-\xi)+\xi(2-\xi)}{[\xi(2-\xi)]^{3/2}}, \tag{19}$$

thus tending to occur earlier as either ε decreases, or ξ increases. This is also shown in Fig. 1 where the vertical lines mark the critical shear rates corresponding to the various cases represented. Expression (19) is an important result which will be derived in a different way from the analysis for the channel and pipe flows presented in the next section.

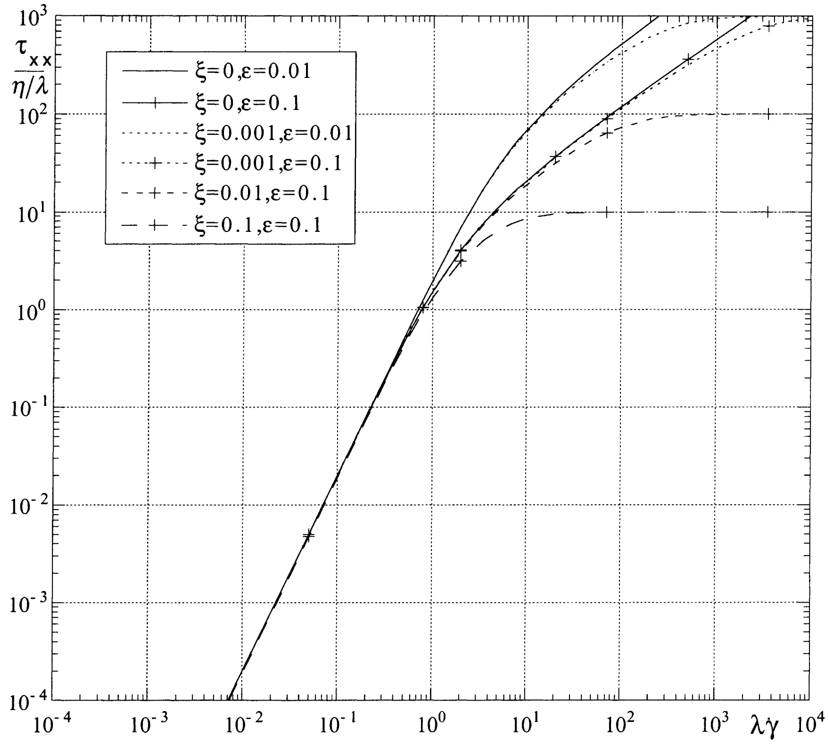

Fig. 2. Variation of the streamwise normal stress with shear rate in steady Couette flow for a PTT fluid with linear stress coefficient.

The corresponding maximum shear stress in plane shear flow is independent of ε, as seen in Fig. 1, and is given by

$$\left(\frac{\tau_{xy}}{\eta/\lambda}\right)_{\max} = \frac{1}{2\sqrt{\xi(2-\xi)}}. \tag{20}$$

The effect of ξ on τ_{xx} is also important and occurs mainly at high shear rates: regardless of the value of ξ, τ_{xx} will tend to a constant value, as shown in Fig. 2, and thus $\Psi_1(\dot{\gamma})$ will vary like $\dot{\gamma}^{-2}$. To this variation there is also a contribution of τ_{yy} but this stress varies in the same way as τ_{xx} as following Eq. (10). As this equation implies τ_{yy} is negative and with ξ taking typically values of 0.2 from experimental data [21], the absolute value of τ_{yy} does not exceed 15% of τ_{xx}, i.e. $|\Psi_2| \leq 0.1|\Psi_1|$.

3. Solution for pipe and channel flows

We deal now simultaneously with the plane and axisymmetric geometries of the channel and pipe flows by introducing a compact notation, with index j being either 0 (channel) or 1 (pipe), and parameter κ being either 3/2 (channel) or 2 (pipe). The channel (pipe) has a half-width (radius) of H, the streamwise coordinate and velocity are x and u, and the cross-stream (radial) coordinate and velocity are y and v, respectively. The coordinate system used is centred ($y = 0$) on the symmetry plane (centreline) and the no-slip condition is valid at the wall ($y = H$). In fully-developed flows the velocity and stresses depend only on the cross-stream coordinate, the pressure gradient $p_{,x}$ is constant and the continuity equation implies a zero transverse velocity ($v = 0$).

The x-momentum equation is independent of the fluid model and can be integrated to give the well-known linear variation of shear stress

$$\boldsymbol{\tau}_{xy} = p_{,x}\frac{y}{2^j}. \tag{21}$$

The constitutive equation reduces to the same set of expressions used in the Couette flow, but it is now more convenient to replace $\dot{\gamma}$ by the velocity gradient $u_{,y}$ as the velocity is one of the variables of interest here. We rewrite Eqs. (7)–(9) as

$$f(\boldsymbol{\tau}_{ii})\boldsymbol{\tau}_{xx} = \lambda(2-\xi)u_{,y}\boldsymbol{\tau}_{xy}, \tag{22}$$

$$f(\boldsymbol{\tau}_{ii})\boldsymbol{\tau}_{yy} = -\lambda\xi u_{,y}\boldsymbol{\tau}_{xy}, \tag{23}$$

$$f(\boldsymbol{\tau}_{ii})\boldsymbol{\tau}_{xy} = \eta u_{,y} + \lambda\left(1-\frac{\xi}{2}\right)u_{,y}\boldsymbol{\tau}_{yy} - \frac{\lambda\xi}{2}u_{,y}\boldsymbol{\tau}_{xx}, \tag{24}$$

with the function $f(\boldsymbol{\tau}_{ii})$ given by Eq. (6). Eq. (10) is still valid and consequently the function $f(\boldsymbol{\tau}_{ii})$ becomes

$$f(\boldsymbol{\tau}_{ii}) = 1 + \frac{2\varepsilon\lambda(1-\xi)}{\eta(2-\xi)}\boldsymbol{\tau}_{xx}. \tag{25}$$

Division of Eq. (24) by Eq. (22) results in a second order equation for the streamwise normal stress

$$\lambda\xi\boldsymbol{\tau}_{xx}^2 - \eta\boldsymbol{\tau}_{xx} + \lambda(2-\xi)\boldsymbol{\tau}_{xy}^2 = 0, \tag{26}$$

which has two possible solutions. However, only one solution is physically realistic: on the symmetry plane ($y = 0$) the x-momentum balance (Eq. (21)) shows the shear stress to be zero which implies $\boldsymbol{\tau}_{xx} = 0$ from Eq. (22). This condition implies that the solution to Eq. (26) is the one with the minus sign before the discriminant, i.e.

$$\boldsymbol{\tau}_{xx} = \frac{\eta}{2\lambda\xi}\left[1-\sqrt{1-\frac{4\lambda^2\xi(2-\xi)\boldsymbol{\tau}_{xy}^2}{\eta^2}}\right]. \tag{27}$$

It is convenient at this stage to introduce a new parameter for compactness

$$a \equiv \frac{-2^{1-j}\lambda p_{,x}H}{\eta}\sqrt{\xi(2-\xi)}, \tag{28}$$

and with the shear stress given by Eq. (21), we obtain

$$\boldsymbol{\tau}_{xx} = \frac{\eta}{2\lambda\xi}\left[1-\sqrt{1-(ay')^2}\right], \tag{29}$$

where $y' \equiv y/H$ is the dimensionless cross-stream coordinate. In fully-developed flow the pressure gradient is negative and since $\xi \leq 2$ we conclude that the dimensionless parameter a is real and positive.

Besides the result itself, the relevance of Eq. (29) is that it indicates the need for $ay' \leq 1$ in order to obtain a real solution for normal stress. This issue will be addressed in Section 4 and, for the moment, it suffices to accept the need for $a \leq 1$.

Expressions for the normalised stress components are useful and are readily obtained after scaling with the wall shear stress for Newtonian (or UCM) fluid. Several well-known non-dimensional numbers will appear in the process, namely the Reynolds and the Deborah numbers. The Reynolds number is only required to express the friction factor in a conventional way and will be here defined as $Re = 2^j \rho UH/\eta$. Viscoelasticity is usually assessed through the Deborah number, here defined as $De = \lambda U/H$ where U is the cross-sectional average velocity in the duct (pipe or channel). The three non-zero normalised stresses become

$$T_{xx} \equiv \frac{\boldsymbol{\tau}_{xx}}{2\kappa\eta U/H} = \frac{1-\sqrt{1-(ay')^2}}{4\kappa De\xi}, \tag{30a}$$

$$T_{yy} \equiv \frac{\boldsymbol{\tau}_{yy}}{2\kappa\eta U/H} = -\frac{1-\sqrt{1-(ay')^2}}{4\kappa De(2-\xi)}, \tag{30b}$$

$$T_{xy} \equiv \frac{\boldsymbol{\tau}_{xy}}{2\kappa\eta U/H} = -\frac{ay'}{4\kappa De\sqrt{\xi(2-\xi)}}. \tag{30c}$$

The whole stress field given by Eqs. (21), (27) and (10), for $\boldsymbol{\tau}_{xy}$, $\boldsymbol{\tau}_{xx}$ and $\boldsymbol{\tau}_{yy}$, respectively, can be substituted into Eq. (22) to give an expression for the transverse variation of the shear rate, which may then be integrated to yield the velocity profile. In order to improve the readability of the equations we introduce another parameter χ which combines ε and ξ in a significant way

$$\chi \equiv \frac{\xi(2-\xi)}{\varepsilon(1-\xi)}, \tag{31}$$

so that the transverse profile of shear rate may be written as

$$\dot{\gamma} = \frac{\mathrm{d}u}{\mathrm{d}y} = \frac{2^{j-1}\eta}{\lambda^2\xi(2-\xi)p_{,x}H}\left[\left(1+\frac{2}{\chi}\right)\left(\frac{1}{y'}-\frac{\sqrt{1-(ay')^2}}{y'}\right)-\frac{a^2y'}{\chi}\right], \tag{32a}$$

or, in non-dimensional form as

$$\Gamma(y') \cong \frac{\dot{\gamma}}{2\kappa U/H} = \frac{-1}{2\kappa De\sqrt{\xi(2-\xi)}}\left[\left(1+\frac{2}{\chi}\right)\left(\frac{1}{ay'}-\frac{\sqrt{1-(ay')^2}}{ay'}\right)-\frac{ay'}{\chi}\right]. \tag{32b}$$

The variation of the viscosity across the duct can be determined from its definition

$$\mu(\dot{\gamma}) \equiv \frac{\boldsymbol{\tau}_{xy}}{\dot{\gamma}} \Rightarrow \frac{\mu(\dot{\gamma})}{\eta} = \frac{a^2y'}{2\left\{(1+2/\chi)\left(1/y'-\left(\sqrt{1-(ay')^2}\right)/y'\right)-(a^2y'/\chi)\right\}}, \tag{33}$$

and finally, the shear rate profile can be integrated to yield the dimensional velocity profile

$$u(y) = \frac{2^{j-1}\eta}{\lambda^2\xi(2-\xi)p_{,x}} \times\left[1+\frac{2}{\chi}\right]\left\{\ln\frac{1+\sqrt{1-(ay')^2}}{1+\sqrt{1-a^2}}+\sqrt{1-a^2}-\sqrt{1-(ay')^2}\right\}+\frac{p_{,x}H^2}{2^j\eta\chi}(1-y'^2). \tag{34}$$

Expression (34) represents a fully analytical solution to the problem of the flow of the complete PTT fluid model through a pipe or channel and it requires knowledge of the applied pressure gradient $p_{,x}$. Often it is the flow rate, or the bulk velocity U, which is known and then it is more convenient to work with the non-dimensional form of Eq. (34) obtained after division by U

$$\frac{u(y)}{U} = -\frac{4\kappa}{a^2}\frac{U_N}{U}\left[1+\frac{2}{\chi}\right]\left\{\ln\frac{1+\sqrt{1-(ay')^2}}{1+\sqrt{1-a^2}}+\sqrt{1-a^2}-\sqrt{1-(ay')^2}\right\}-\frac{2\kappa}{\chi}\frac{U_N}{U}[1-y'^2]. \tag{35}$$

In this equation the parameter U_N is defined by

$$U_N \equiv -\frac{p_{,x}H^2}{2^{j+1}\kappa\eta} \tag{36}$$

and represents the bulk velocity for the flow of a Newtonian fluid subjected to the same pressure gradient. The ratio U_N/U can also be viewed as a dimensionless pressure gradient and, for this case of given U, it is a new unknown of the problem. It can be obtained from integration of the velocity profile over the duct cross-section, as a result of the standard definition of the bulk velocity

$$U \equiv \frac{1}{H^{j+1}}\int_0^H 2^j y^j u(y)\,\mathrm{d}y. \tag{37}$$

This integration leads to different expressions for the channel flow case

$$\left(\frac{U_N}{U}\right)^{-1} = \frac{6}{a^2}\left[1+\frac{2}{\chi}\right]\left\{1-\frac{\pi}{4a}+\frac{1}{2a}\arctan\left(\frac{\sqrt{1-a^2}}{a}\right)-\frac{\sqrt{1-a^2}}{2}\right\}-\frac{2}{\chi}, \tag{38a}$$

and for the pipe flow case

$$\left(\frac{U_N}{U}\right)^{-1} = \frac{4}{a^2}\left[1+\frac{2}{\chi}\right]\left\{1-\frac{2}{3}\sqrt{1-a^2}-\frac{2}{3}\frac{(1-\sqrt{1-a^2})}{a^2}\right\}-\frac{2}{\chi}. \tag{38b}$$

It is important to realise that Eqs. (38) do not provide, however, an explicit expression for U_N/U since a itself depends on U_N/U as a comparison of Eq. (28) for a and Eq. (36) for U_N shows. In fact, it is easy to show that a and U_N/U are related by

$$a = 4\kappa\frac{U_N}{U}De\sqrt{\varepsilon(1-\xi)}\sqrt{\chi}, \tag{39}$$

and this expression suggests that we take as two independent parameters a modified Deborah number (defined by $De^* \equiv De\sqrt{\varepsilon(1-\xi)}$) and χ (defined in Eq. (31)). These parameters are only unsuitable in the limiting case of $\varepsilon = 0$, when the standard JS fluid is recovered and where one has to revert back to De and ξ.

Hence, Eqs. (38a) and (38b) represent two highly non-linear functions of two non-dimensional parameters

$$\frac{U_N}{U} = \mathrm{function}(De^*, \chi), \tag{40}$$

which must be solved for U_N/U by numerical means. To this aim we have used a straightforward bisection method and the solution is represented in graphical form to be given and discussed in the next section.

In engineering calculations involving polymer flows in ducts one is often interested in determining pressure drop and pumping capacity, and for this we need an expression for *fRe*, where *f* is the Fanning friction factor usually defined as $f \equiv -2^{1-j} p_{,x} H/\rho U^2$. Using the definition of Reynolds number given above and after some algebra, we arrive at the following expression for *fRe*:

$$f Re = 2^{j+2}\kappa \frac{U_N}{U}. \tag{41}$$

This shows that the variation of *fRe* with *De*, ε and ξ is proportional to the corresponding variation of the parameter U_N/U and so there is no need to study *fRe* separately.

4. Constitutive flow instability

A real solution for the streamwise normal stress (Eq. (29)) was subjected to the condition that $ay' \leq 1$, and since y' varies between 0 and 1

$$ay' \leq 1 \Rightarrow a \leq 1. \tag{42}$$

As we shall see, the equality $a = 1$ leads to a condition corresponding to the onset of a constitutive instability akin to that found for the JS model and investigated in detail by Español et al. [19] and Georgiou and Vlassopoulos [20]. For this reason we will refer to that condition as representative of “flow instability” even though we cannot offer a physical interpretation for the actual resulting flow; the flow may become unstable and time-dependent, or it may happen that no solution exists.

We start by determining the maximum shear rate in the duct cross-section, which takes place at the wall, i.e. $y = H$. We denote $\dot{\gamma}_{\max} \equiv |\dot{\gamma}_{y=H}|$ and from Eq. (32a) we obtain

$$\dot{\gamma}_{\max} = \frac{-\eta}{2^{1-j}\lambda^2\xi(2-\xi)p_{,x}H}\left[\left(1+\frac{2}{x}\right)\left(1-\sqrt{1-a^2}\right)-\frac{a^2}{\chi}\right]. \tag{43}$$

Note the minus sign leading the equation to produce a positive shear rate at the wall. Now, we impose the limiting stability condition $a = 1$ together with Eq. (28) to obtain

$$\dot{\gamma}_{\max,c} = \frac{1}{\lambda\sqrt{\xi(2-\xi)}}\left[1+\frac{1}{\chi}\right], \tag{44}$$

and finally

$$\lambda\dot{\gamma}_{\max,c} = \frac{1+(1/\chi)}{\sqrt{\xi(2-\xi)}} \Leftrightarrow \lambda\dot{\gamma}_{\max,c} = \frac{\varepsilon(1-\xi)+\xi(2-\xi)}{[\xi(2-\xi)]^{3/2}}, \tag{45}$$

which is the same equation presented in Section 2 for $\lambda\dot{\gamma}_c$. Hence, we find that the critical shear rate for the maximum of the curve $\boldsymbol{\tau}_{xy}$ versus $\dot{\gamma}$ in a simple shear flow ($\dot{\gamma}_c$) is the same as the maximum allowable shear rate in a duct flow with imposed pressure gradient ($\dot{\gamma}_{\max,c}$). Above this maximum shear rate, the governing equations for the duct flow do not have a real solution. The constitutive instability due to non-monotonic shear stress in simple shear is thus connected with conditions for an imaginary solution in the more complex duct flow.

In his 1958 paper, Oldroyd [22] studied the behaviour of the now known as the eight-constant Oldroyd model, with view to determine the model parameters that result in predictions of real flow behaviour, such as an apparent viscosity being a decreasing function of the shear rate (his Eq. (54)). This is related, but not equivalent, to studies of flow stability like that of Yerushalmi et al. [23], who have considered the corotational Maxwell model (CRM) with and without a retardation time (or, with and without a Newtonian solvent contribution). Yerushalmi et al. [23] have found that flow instability sets in whenever the slope of the flow curve is negative and, for the pure CRM, that happened for shear rates in excess of a critical value whereas for the corotational Jeffreys model (equivalent to CRM plus a Newtonian solvent), it occurred within a range of shear rates limiting a local maximum and a local minimum in the corresponding flow curve. Thus, the addition of a Newtonian solvent imparts a second critical shear rate at the point where the shear stress exhibits a local minimum. In both cases we are in the presence of constitutive flow instabilities. In the present study we have not, however, the effect of a solvent viscosity.

More recently, these issues have been revived because of the possible link with instabilities found in polymer processing flows. It is the case of the spurt phenomena studies of Kolkka et al. [13] and the investigations of shear banding by Español et al. [19] and Georgiou and Vlassopoulos [20]. In these three works the constitutive equation was the JS model with an added Newtonian viscosity which imparts the second higher critical shear rate associated with the local minimum in shear stress. Although the derivatives used in the CRM and JS constitutive equations are different, the JS fluid suffers from the same shortcomings as the CRM model, hence the effect of adding the retardation time results in the same instability phenomena, leading to the so-called shear banding. The shear banding instabilities exist in this limited range of shear rates where there are multiple solutions to the relationship between the shear rate and shear stress and where the former is a decreasing function of the latter.

In the present work, no retardation time term was added to the PTT model, so there is a single maximum in the shear stress–shear rate curve. If the imposed pressure gradient is such that the wall shear stress exceeds the maximum value, given by Eq. (20), there is no real solution to the steady Poiseuille flow, which may be equivalent in physical terms to the appearance of a different flow, possibly an unsteady flow. Note that the JS model is recovered from the complete PTT model if $\varepsilon = 0$, so our findings and the works of Yerushalmi et al. [23], Kolkka et al. [13], Español et al. [19] and Georgiou and Viassopoulos [20] suggest that shear banding would also occur for the full PTT fluid with added Newtonian solvent.

Since the constitutive instability is associated with the maximum in the shear stress–shear rate relationship it will always be potentially there provided ξ is non-zero as Fig. 1 has already shown. Fig. 3 represents the normalised critical shear rate as a function of ξ and ε and shows the stability condition to occur at lower values of the shear rate, as ξ increases and ε decreases. When ξ goes to zero (absence of lower convected derivative in the constitutive equation), $\dot{\gamma}_{\mathrm{max,c}}$ tends to infinity and the flow will be always stable from a constitutive point of view, as found in our previous work [6]. Similarly, the presence of a non-vanishing ε, which brings in some extra degree of shear-thinning to the pure JS fluid, tends to promote stability as the inception of unstable constitutive behaviour is shifted to higher values of shear rate. This parameter ε does not play, however, any role in terms of defining the critical pressure gradient, which is given by

$$\frac{(-p_{,x})_{\mathrm{c}}H}{\eta/\lambda} = \frac{1}{2^{1-j}\sqrt{\xi(2-\xi)}}, \tag{46}$$

rather it acts upon the shape of the velocity profile, making it flatter in the core and steeper at the wall.

Constitutive stability, however, does not preclude the existence of flow instabilities as is known from the fluid mechanics of Newtonian fluids. For viscoelastic fluids, for instance, Baaijens [24] reported instabilities for the SPTT fluid in Couette and Poiseuille flows when the stress function was exponential.

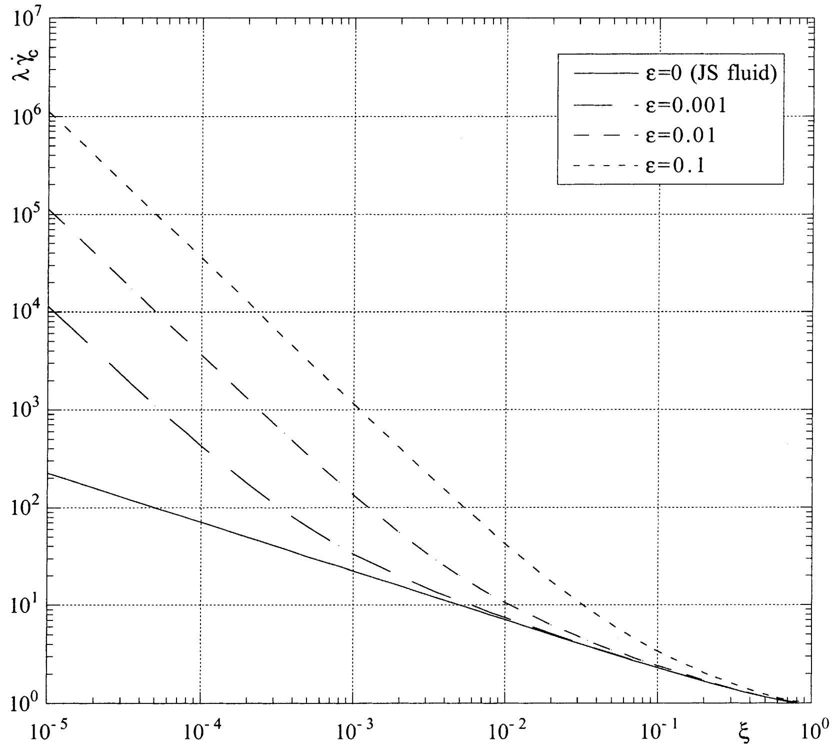

Fig. 3. Variation of the critical shear rate with the material parameters ε and ξ.

Constitutive instabilities will also have an influence on the behaviour of multi-mode viscoelastic fluids, but the different weights of the various modes on the total stress will certainly result in a different, probably wider, range of stability conditions.

The above "stability" condition can also be recast in a different way, involving bulk flow quantities and non-dimensional numbers. This results in expressions which are most illuminating for a physical understanding of the conditions beyond which there are no real solutions to the pipe and channel flow problems. Eq. (40) states that the pressure drop for a given flow rate, U_N/U, depends on two parameters, De^* and χ. At the limiting "stability" point the additional condition (42) implies that there remains only a single independent parameter which we may take as De^* or χ whichever is more convenient. For the plane case of channel flow, if we equate Eqs. (38a) and (39), subjected to the stability restraint (42), we arrive at

$$\left(\frac{U}{U_N}\right)_{\mathrm{c}}\sqrt{\frac{1}{(10-3\pi)}\left[\left(\frac{U}{U_N}\right)_{\mathrm{c}}-6\left(1-\frac{\pi}{4}\right)\right]}=6De_{\mathrm{c}}^{*}, \tag{47}$$

where De_{c}^* and $(U_N/U)_{\mathrm{c}}$ denote critical values of De^* and U_N/U separating the zones of allowable and imaginary solutions. If we plot Eq. (47) in a graph of U_N/U versus De^* we obtain the thick line in Fig. 4. This representation can be viewed as a stability map since the region below the thick line (Eq. (47)) does not allow for any real solution ("unstable region") and the admissible solutions must be located above that line ("stable region"). In terms of the effect of ξ and ε, an increase in ξ reduces the velocity ratio and narrows the range of permissible solutions whereas increasing ε tends to stabilise the flow.

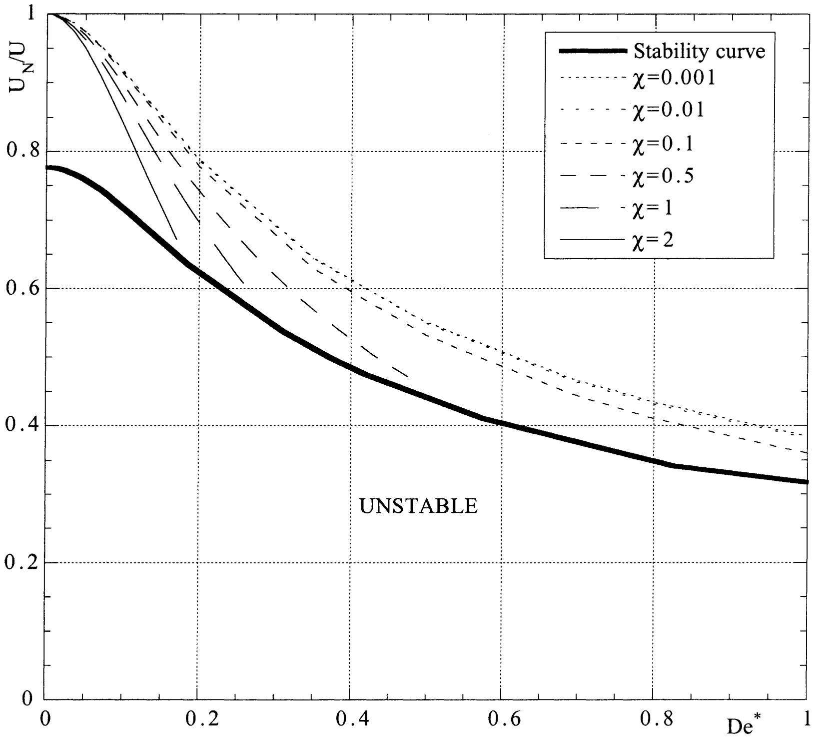

Fig. 4. Stability map of the PTT model fluid and ratio of Newtonian and PTT bulk velocities as a function of De^* and χ for channel flow.

When De^* tends to zero (negligible elasticity), the critical velocity ratio (or pressure drop) tends to $(U_N/U)_c \to 1/6(1-\pi/4) \approx 0.7766$. On the other extremity, as $De^* \to \infty$ $(U_N/U)_c$ asymptotes to zero. It is also useful to check the limit $\varepsilon \to 0$ which brings the full PTT model equal to the JS model ($\chi \to \infty$) and allows comparison with results of Kolkka et al. [13] for the case without added Newtonian solvent. To do this for the channel flow, we express De_c^* in terms of χ as

$$De_c^* = \frac{1}{\sqrt{\chi}}\left[\left(1-\frac{\pi}{4}\right)+\frac{1}{3\chi}\left(5-\frac{3}{2}\pi\right)\right], \qquad (48)$$

and since in this limiting condition it is more adequate to use the standard Deborah number, we introduce the definition of χ (Eq. (31)) to get

$$De_c = \frac{1}{\sqrt{\xi(2-\xi)}}\left[\left(1-\frac{\pi}{4}\right)+\frac{1}{3\chi}\left(5-\frac{3}{2}\pi\right)\right]. \qquad (49)$$

Now, $\chi \to \infty$ gives $De_c = (1-\pi/4)/\sqrt{\xi(2-\xi)}$ which is equal to the result of [13]. In their paper, the critical Weissenberg number is given by their Eq. (33) $We_c = (1-\ln 2)/\sqrt{1-c^2}$, with $c = 1-\xi$, where $We \equiv \lambda U_0/H$ is defined with the maximum centreline velocity U_0. From our velocity profile (Eq. (35)) with $a = 1$ and $\chi \to \infty$ we obtain the ratio $U_0/U = (1-\ln 2)/(1-\pi/4)$, that allows the direct comparison between our definition of *De* and theirs of *We*.

For the pipe flow case, a similar derivation leads to a critical curve separating the stable and unstable regions given by

$$\left(\frac{U}{U_N}\right)_{\mathrm{c}}\sqrt{\frac{3}{2}\left(\frac{U}{U_N}\right)_{\mathrm{c}}-2}=8De_{\mathrm{c}}^{*} \tag{50}$$

When $De^{*}\to 0$, the critical pressure drop tends to $(U_N/U)_{\mathrm{c}}\to 3/4$. In terms of χ, the critical Deborah number may be written as

$$De_{\mathrm{c}}^{*}=\frac{1}{6\sqrt{\chi}}\left[1+\frac{1}{2\chi}\right], \tag{51}$$

and for the limiting condition leading to the JS model ($\varepsilon\to 0$, $\chi\to\infty$) we obtain $De_{\mathrm{c}}=1/6\sqrt{\xi(2-\xi)}$. In the other limit $\xi\to 0$, $De_{\mathrm{c}}\to\infty$, i.e. the flow is always stable, as expected.

The variation of the modified critical Deborah number with χ is given in Fig. 5, for both the channel (Eq. (48)) and pipe flow cases (Eq. (51)). Each point in these curves corresponds therefore to the De^{*} resulting from the intersection of the permissible U_N/U versus De^{*} solutions in Fig. 4 with the thick stability curve. Fig. 5 makes it clear that the range of *De* for a stable flow becomes wider and wider as χ is reduced, that is as the elongational ε parameter of the PTT model is increased and/or the slip parameter is decreased.

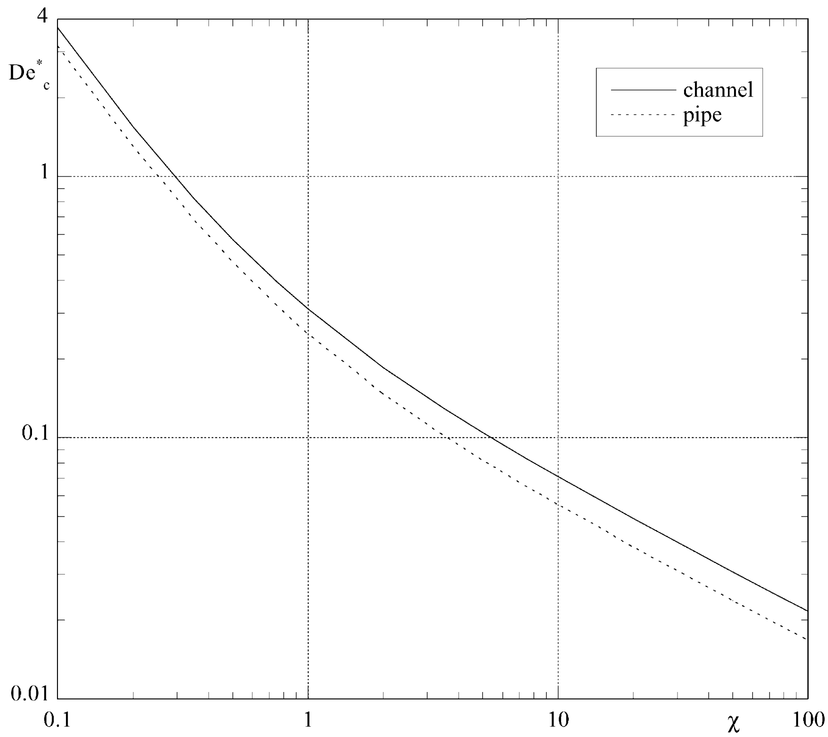

Fig. 5. Variation of the modified critical Deborah number with parameter χ for channel and pipe flows.

5. Discussion of the steady pipe and channel flow results

Within the constitutive stable flow region, the thin lines in Fig. 4 show the variation of U_N/U with the Deborah number, with χ taken as parameter. The shear-thinning behaviour of the PTT fluid tends to lower the viscosity near the wall compared with the Newtonian fluid and, consequently, for identical pressure

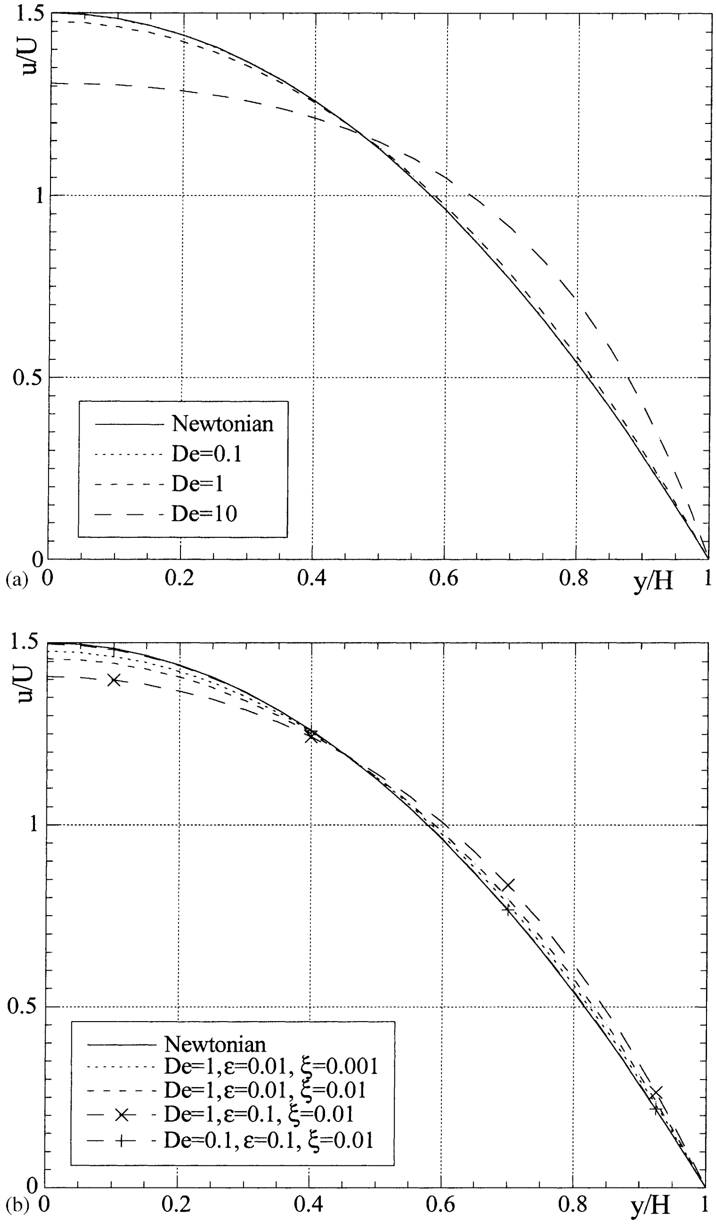

Fig. 6. Transverse profiles of axial velocity for channel flow. (a) Effect of Deborah number ($\varepsilon = 0.01$, $\xi = 0.001$); (b) effect of ε and ξ.

gradient the flow rate of the PTT fluid will be higher, i.e. the ratio U_N/U drops with the parameters that enhance shear-thinning, *De* and χ.

As the ratio U_N/U decreases due to increased shear-thinning the velocity profiles become flatter as shown in the representative plots of Fig. 6. The corresponding profiles for the normalised stresses are shown in Figs. 7–9, for the shear, streamwise normal and cross-stream normal components, respectively.

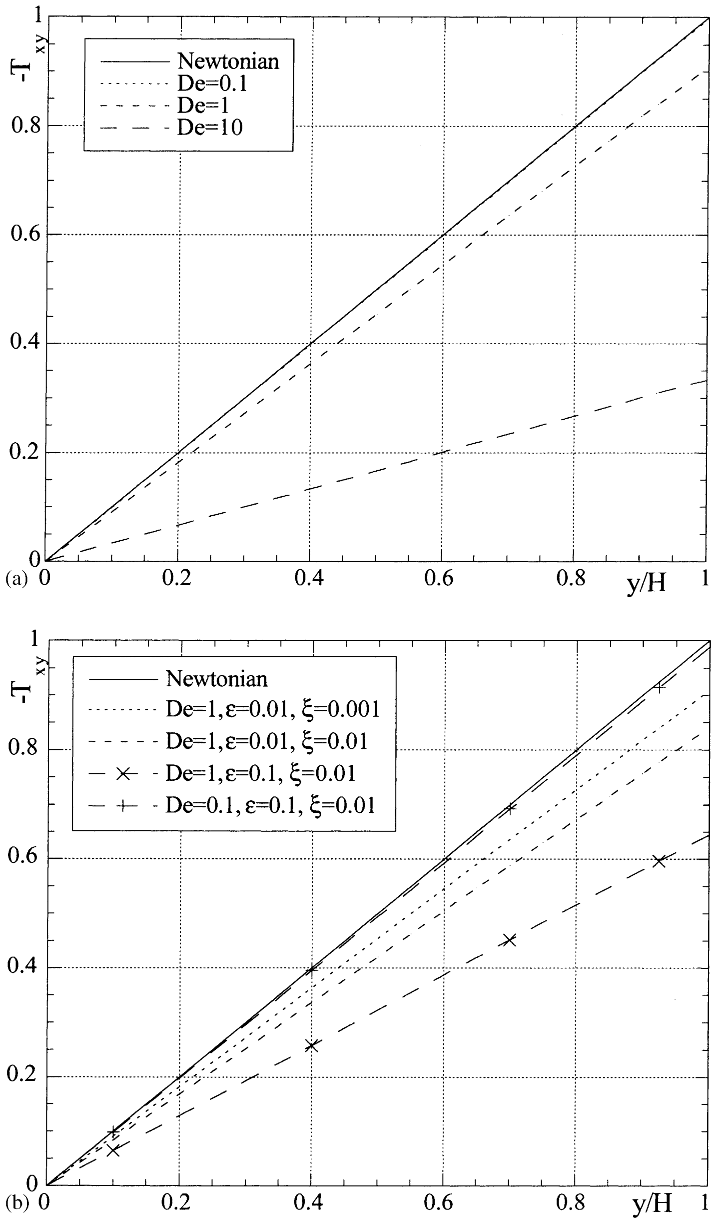

Fig. 7. Transverse profiles of shear stress for channel flow. (a) Effect of Deborah number ($\varepsilon = 0.01$, $\xi = 0.001$); (b) effect of ε and ξ.

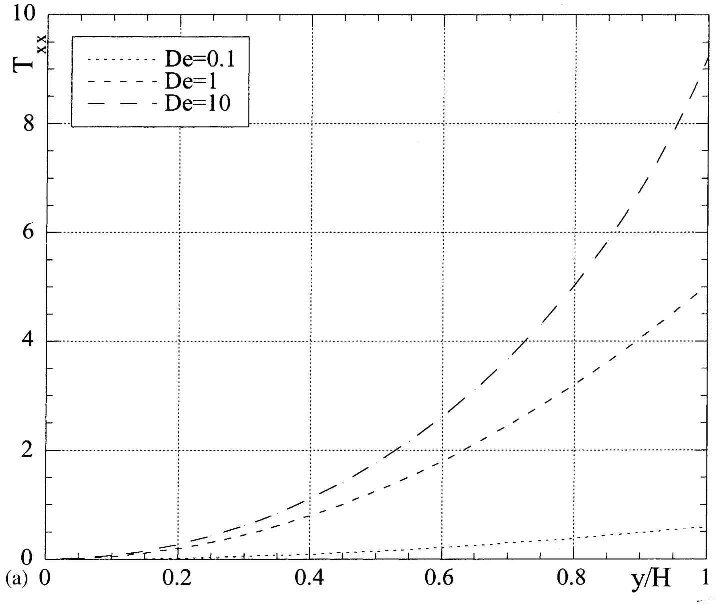

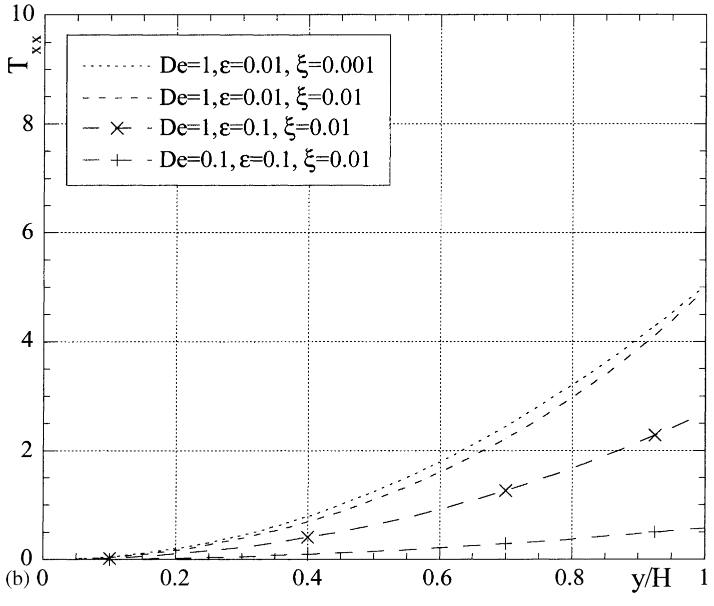

Fig. 8. Transverse profiles of streamwise normal stress for channel flow. (a) Effect of Deborah number ($\varepsilon = 0.01$, $\xi = 0.001$); (b) effect of ε and ξ.

The profiles in Figs. 6–9 could have been plotted in a simpler way using the modified Deborah number De^* as abcissa, and χ as the parameter, like in Fig. 4, but we preferred to investigate separately the effects of the model constants ε and ξ.

The shear stress across the gap must follow a linear variation irrespective of the constitutive equation but its magnitude depends on the model parameters. As seen above, increasing levels of shear-thinning

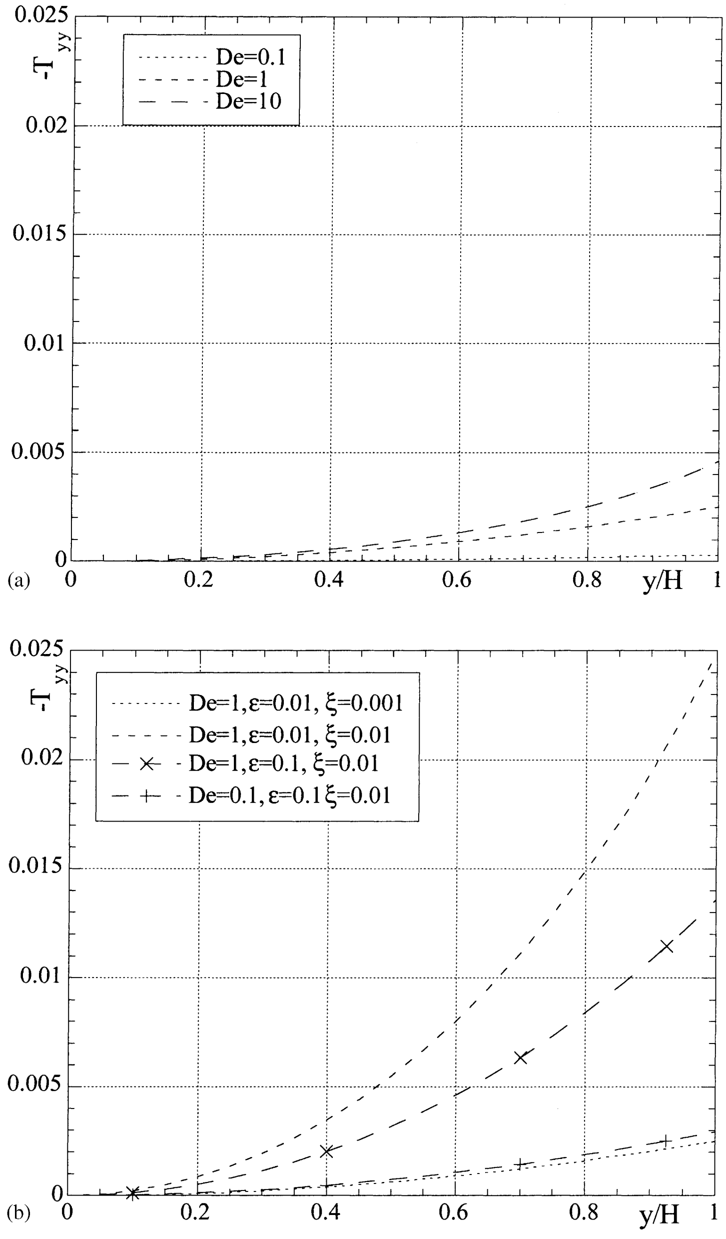

Fig. 9. Transverse profiles of cross-stream normal stress for channel flow. (a) Effect of Deborah number ($\varepsilon = 0.01$, $\xi = 0.001$); (b) effect of ε and ξ.

increase the flatness of the velocity profiles and the wall shear rate, thus reducing the wall viscosity and generally leading to a smaller wall shear stress, or pressure gradient for identical bulk velocity. In this respect, it is noted, from Eqs. (30c) and (39), that the dimensionless wall shear stress is equal to $T_\mathrm{w} \equiv |T_{xy}(y=1)| = U_N/U$, whose variation was given in Fig. 4. The three parameters ε, ξ and λ, the latter via *De*, all contribute to lower values of $|T_{xy}|$.

The picture is different for the two normal stresses. With T_{xx} in Fig. 8, we see that both ε and ξ contribute to its reduction, with ε imparting a stronger effect than ξ. On the other hand, increasing levels of viscoelasticity (higher *De*) increases this stress component. The transverse normal stress T_{yy} plotted in Fig. 9, is the product of the axial normal stress and a multiplier based on ξ (Eq. (10)). It happens that the effect of ξ upon the multiplier is opposite and much stronger to that upon T_{xx} and consequently T_{yy}

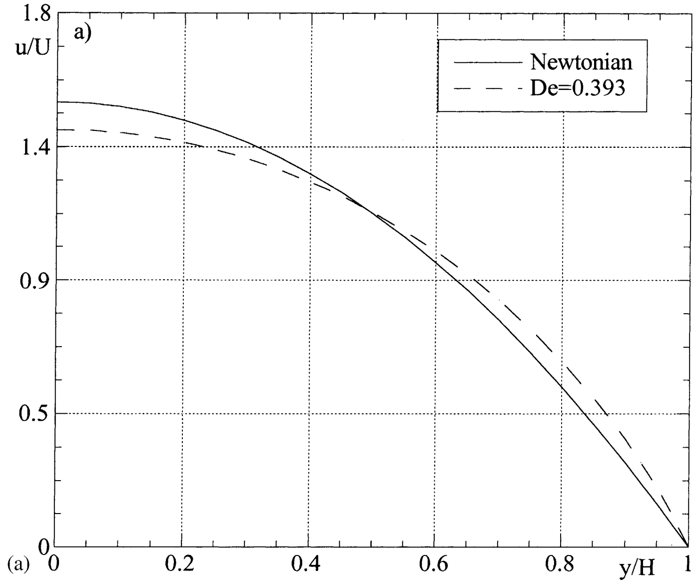

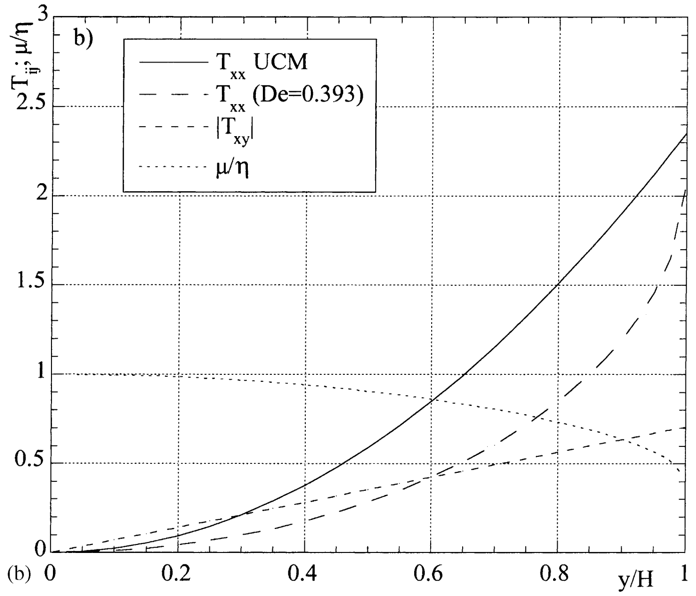

Fig. 10. Transverse profiles in channel flow for conditions just below critical at $De = 0.393$ with $\xi = 0.2$ and $\varepsilon = 0.1$: (a) velocity; (b) stresses and viscosity.

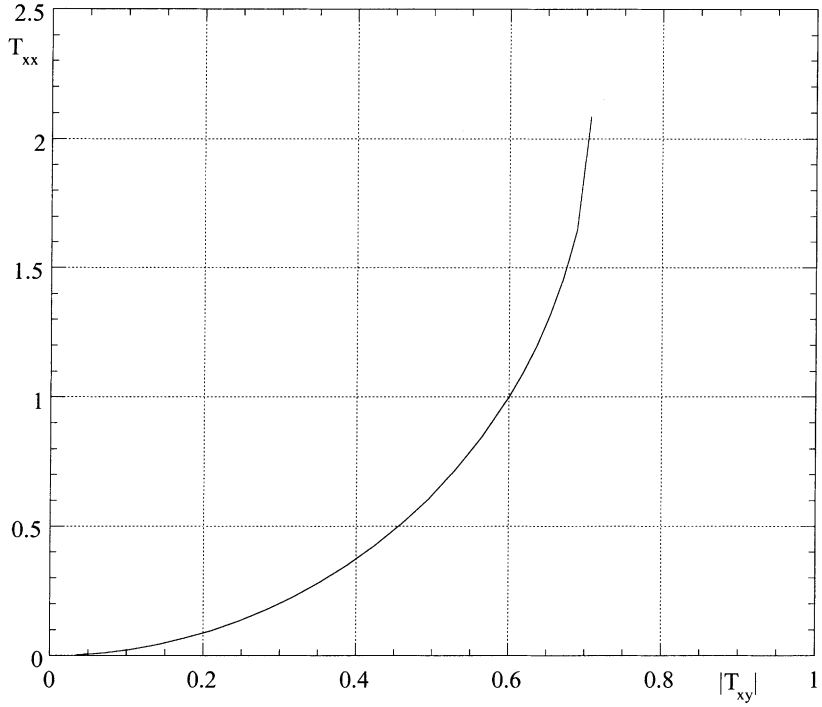

Fig. 11. Variation of the normal stress with shear stress across the channel for a situation just below critical ($\xi = 0.2$, $\varepsilon = 0.1$, $De = 0.393$).

increases with ξ whereas T_{xx} decreased. Common to all the stresses is the finding that the effects of ε, ξ and De are proportional to the value of De: for small values of De, say $De \leq 0.1$, Figs. 7b–9b show very small variations of the stresses with parameters ε and ξ.

It is interesting to observe the resulting profiles for a situation on the verge of a critical state. For typical values of the parameters $\xi = 0.2$ and $\varepsilon = 0.1$, which correspond to $\chi = 4.5$, the critical state in channel flow is at a modified Deborah number of $De_c^* = 0.11121$ ($De_c = 0.39318$) according to Eq. (48). The value $De = 0.393$ ($De_c^* \approx 0.11116$) is just below critical and Fig. 10 shows that, although the velocity profile seems absolutely normal, the normal stress T_{xx} is seen to increase sharply near the wall. If the stress components were plotted versus the local shear rate it would be readily apparent that while T_{xx} would grow almost linearly with $\dot{\gamma}$, T_{xy} would tend to level out showing a maximum near the wall, in agreement with the results for the simple shear flow of Section 2. This differentiated rate of growth of the normal and shear stresses is, however, much clearer if we plot one versus the other, as in Fig. 11. Now we see that the critical situation corresponds to a slope of T_{xx} with T_{yy} tending to infinity; this finding could have been foreseen from Eq. (27), for if we do $(\partial \boldsymbol{\tau}_{xx}/\partial \boldsymbol{\tau}_{xy}) \to \infty$, we obtain the critical condition under the form of Eq. (46).

6. Conclusions

Analytical solutions are derived for the laminar steady channel and pipe flows of PTT fluids with the linear stress coefficient and without solvent viscosity. The results include the profiles of all relevant stresses, the axial velocity and the viscosity across the gap. Expressions are also given for the viscometric viscosity and the first and second normal stress difference coefficients, as a function of the shear rate, in steady plane shear flow. Similarly to the JS fluid, the shear stress was found not to be a monotonically increasing function of the shear rate as strong shear-thinning sets in. The critical condition for the maximum in the shear stress–shear rate rheogram is presented.

The two duct flows are found to be unstable when the pressure gradient exceeds a critical value, determined by a maximum shear rate at the wall, and this condition, of constitutive origin, was found to be related to the critical condition in the simple shear flow. The inter-relation between the critical Deborah number in duct flow, the critical pressure drop (or U_N/U, or wall shear stress) and the modified model parameter χ, was established and discussed. A stability map for channel and pipe flows was given.

The expressions derived for the pipe and channel flows allowed the assessment and discussion of the effects of ε, ξ and De upon the flow hydrodynamics.

References

[1] N. Phan-Thien, R.I. Tanner, A new constitutive equation derived from network theory, J. Non-Newtonian Fluid Mech. 2 (1977) 353–365.

[2] N. Phan-Thien, A non-linear network viscoelastic model, J. Rheol. 22 (1978) 259–283.

[3] R.I. Tanner, R.R. Huilgol, Rheol. Acta 14 (1975) 959–962.

[4] R.G. Larson, Constitutive Equations for Polymer Melts and Solutions, Butterworths, Boston, 1988.

[5] Z. Tadmor, C.G. Gogos, Principles of Polymer Processing, 1st Edition, Wiley, New York, 1979.

[6] P.J. Oliveira, F.T. Pinho, Analytical solution for fully-developed channel and pipe flow of Phan-Thien–Tanner fluids, J. Fluid Mech. 387 (1999) 271–280.

[7] F.T. Pinho, P.J. Oliveira, Analysis of forced convection in pipes and channels with the simplified Phan-Thien–Tanner fluid, Int. J. Heat Mass Transfer 43 (2000) 2273–2287.

[8] F.T. Pinho, P.J. Oliveira, Axial annular flow of a non-linear viscoelastic fluid: an analytical solution, J. Non-Newtonian Fluid Mech. 93 (2000) 325–337.

[9] H.C. Choi, J.H. Song, J.Y. Yoo, Numerical simulation of the planar contraction flow of a Giesekus fluid, J. Non-Newtonian Fluid Mech. 29 (1988) 347–379.

[10] F.J. Lim, W.R. Schowalter, Pseudo-spectral analysis of the stability of pressure-driven flow of a Giesekus fluid between parallel planes, J. Non-Newtonian Fluid Mech. 26 (1987) 135–142.

[11] G. Schleiniger, R.J. Weinacht, Steady Poiseuille flows for a Giesekus fluid, J. Non-Newtonian Fluid Mech. 40 (1991) 79–102.

[12] J.A. Deiber, A.S.M. Santa Cruz, On non-Newtonian fluid flow through a tube of circular cross-section, Lat. Am. J. Chem. Eng. Appl. Chem. 14 (1984) 19–38.

[13] R.W. Kolkka, D.S. Malkus, M.G. Hansen, G.R. Ierley, R.A. Worthing, Spurt phenomena of the Johnson–Segalman fluid and related models, J. Non-Newtonian Fluid Mech. 29 (1988) 303–335.

[14] J.J. Van Schaftingen, M.J. Crochet, Analytical and numerical solution of the Poiseuille flow of a Johnson–Segalman fluid, J. Non-Newtonian Fluid Mech. 18 (1985) 335–351.

[15] R.K. Shah, A.L. London, Laminar Flow Forced Convection in Ducts, Academic Press, New York, 1978.

[16] R.B. Bird, R.C. Armstrong, O. Hassager, Dynamics of Polymeric Liquids, Fluid Dynamics, 2nd Edition, Vol. 1, Wiley, New York, 1987.

[17] A.H.P. Skelland, Non-Newtonian Flow and Heat Transfer, Wiley, New York, 1967.

[18] S.-C. Xue, N. Phan-Thien, R.I. Tanner, Three-dimensional numerical simulations of viscoelastic flows through planar contractions, J. Non-Newtonian Fluid Mech. 74 (1998) 195–245.

[19] P. Español, X.F. Yuan, R.C. Ball, Shear banding flow in the Johnson–Segalman fluid, J. Non-Newtonian Fluid Mech. 65 (1996) 93–109.

[20] G.C. Georgiou, D.V. Vlassopoulos, On the stability of the simple shear flow of a Johnson–Segalman fluid, J. Non-Newtonian Fluid Mech. 75 (1998) 77–97.

[21] R.R. Huilgol, N. Phan-Thien, Fluid Mechanics of Viscoelasticity, Rheology Series, Vol. 6, Elsevier, Amsterdam, 1997.
[22] J.G. Oldroyd, Non-Newtonian effects in steady motion of some idealized elastico–viscous liquids, Proc. Royal Soc. A245 (1958) 278–297.
[23] J. Yerushalmi, S. Katz, R. Shinnar, The stability of steady shear flows of some viscoelastic fluids, Chem. Eng. Sci. 25 (1970) 1891–1902.
[24] F. Baaijens, Stability analysis of viscoelastic flows and application to polymer melt flows, Lecture FB4 of the CIM Summer School "Analytical and Numerical Methods in Non-Newtonian Fluid Mechanics" held at Universidade do Minho, Guimarães, Portugal, 25–29 June 2001.